13.4

High-current field emission nanostructure with a ribbon beam

© M.V. Davidovich

Saratov National Research State University, Saratov, Russia
E-mail: davidovichmv@info.sgu.ru

Received May 15, 2023
Revised March 29, 2024
Accepted May 2, 2024

The issues of the achievability of high current densities of the order 10^{10}-10^{12} A/m^2 and the integral current of a ribbon electron beam of the order $1-10$ A for vacuum electronic devices are considered. A resonant tunneling nanostructure and an electron gun design based on it are proposed.

Keywords: field emission, autocathode, Schrodinger equation, resonant tunneling, ribbon electron beam, TWT.

DOI: 10.61011/TPL.2024.08.58921.19626

High-current electron guns with wide ribbon electron beams [1,2] are needed for traveling wave tubes (TWTs) operating in the millimeter and terahertz ranges. It was demonstrated in [3,4] that current densities up to $10^{12}-10^{13}$ A/m^2 may be achieved in resonant-tunneling nanostructures with one or two quantum wells (grids) and two or three humps (barriers) at structure sizes up to 10 nm and anode and grid voltages up to 20 V. It is convenient to fabricate such nanoscale heterostructures in the form of alternating dielectric and conductive layers with their thickness ranging from 1 to $2-3$ nm. Crystalline diamond with permittivity $\varepsilon = 5.6$ and an exceptionally high thermal conductivity is the optimum dielectric material. It is technologically convenient to use CVD (chemical vapor deposition) carbon, in particular amorphous diamond with an sp^3 bond fraction up to 88% [5–7], as a dielectric and highly conductive carbon with predominant sp^2 hybridization as metallic layers. Specifically, six-layer graphene has a thickness of 2 nm. The permittivity of amorphous diamond is $4.8-5.6$. The barriers are then lowered by a factor of approximately 5. In a diode structure, this raises the current by 2–4 orders of magnitude (depending on the barrier height). In a resonant-tunneling structure, this allows one to achieve a several-fold reduction in anode voltage. Another possibility is the use of thicker films. A thin film is metallic if Debye screening length $L_D = \sqrt{\varepsilon\varepsilon_0 k_B T/N}/e$ is significantly smaller than its thickness. In semiconductors with a carrier density of $N \sim 10^{20}-10^{24}$ m^{-3}, screening occurs at distances from 1 to 100 nm; in metals, over a single atomic layer. Densities higher than 10^{24} m^{-3} correspond to metallic properties at a thickness of 1 nm. Specifically, $L_D = 1.5 \cdot 10^{-11}$ m for copper. A high ribbon beam current may be obtained from a large emitting surface, but beam compression is required. It is also possible to use trajectory rotation [8]. The beam current then increases with length and width of the emitting structure. Its advantage is that emission proceeds from both sides. The disadvantage of this structure is a high thermal load (due mostly to the Nottingham effect in resonant tunneling, which may be initiated at levels lying significantly lower than the Fermi level, and to Joule heating). A massive thermostat at the cathode and pulsed operation are required in this case. The diagram of a TWT with a slow-wave structure of the symmetrical comb type with the discussed field emission structure is shown in Fig. 1. Trajectories were analyzed in CST Studio Suite. The solution of the 1D Schrödinger equation (SE) with quantum potential $V(s)$ distributed along the trajectories of electrons and with summation over them was used to calculate the current. We assume that the density of electrons moving normally to the grid is uniform. Quantum potential profile $V(s)$ was plotted using the method of multiple images, which was discussed in detail in [2,4,9]. These profiles for different trajectories remain virtually identical up to the transit through the grid region and diverge only after this transit (Fig. 2, *a*; a small part of the change in potential near the electron emission points in Fig. 1 is shown). Following transit, an electron moves between the grid with potential U_g and the first anode with potential U_a and is affected by the image force potential and potential $V_a(s) = -eU_g - e(U_g - U_a)(s - s_0)/d(z)$. In this formula, $s_0 = t_d + t_g$ — size of the cathode structure (t_d is the dielectric material thickness and t_g is the grid thickness), coordinate s is measured along the trajectories, and $d(z)$ — length along the trajectory corresponding to coordinate z of its origin at the cathode. Coordinate s is measured along the motion trajectory; $z = 0$ corresponds to the furthest point (and the maximum trajectory length), while $z = l_c$ corresponds to the nearest point. The image forces are characterized by potential $V_0(s)$, and the overall potential is $V(s) = V_0(s) + V_a(s)$. Let us denote the length of the emitting cathode region as l_c and the cathode–anode distance as l_a; $D(E, z)$ is the transparency (coefficient of tunneling through potential $V(s)$) corresponding to point z. The current density around point z is then

$$J(z) = \frac{em_e}{2\pi^2\hbar^3}\int_0^{E_{Fc}} D(E, z)(E_{Fc} - E)dE. \qquad (1)$$

Here, E_{Fc} is the Fermi energy at the cathode, and the temperature is considered to be zero. If the width of

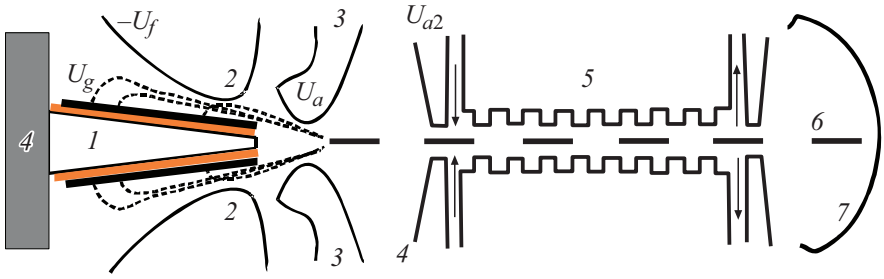

Figure 1. Diagram of a TWT with a ribbon beam. *1* — Cathode with a pulling grid, *2* — focusing electrode, *3* — anode, *4* — cathode thermostat, *5* — second anode with a slow-wave structure of the symmetrical comb type, *6* — ribbon electron beam, and *7* — collector.

the structure (along the normal to the plane of Fig. 1) is w, its total current is $I = 2w\int_0^{l_c} J(z)dz$. Thus, the main task is to determine the transparency for different electron energies E at the cathode and different barrier structure profiles shown in Fig. 2, *a*, which correspond to various trajectories. This is done by solving the SE by the method of transformation of wave impedance $\rho(s) = \pm i\psi_\pm(s)/\psi'_\pm(s)$, where $\psi_\pm(s) = A_\pm \exp(\pm iks)$ are the direct and inverse wave functions constructed for a constant section of potential V. Two fundamental solutions of the SE are given here. Thus, $k(s) = \sqrt{2m_e(E-V)}/\hbar$. At the cathode, the wave number and the impedance are $k_c = \sqrt{2m_eE}/\hbar$ and $\rho_c = 1/k_c$; at the anode, the corresponding parameters are $k_a = \sqrt{2m_e(E - E_{Fa} + eU_a)}/\hbar$ and $\rho_a = 1/k_a$. The transformation of wave impedance ρ_a at the anode to input impedance Z_{in} at the cathode with the impedance transformation formula yields the following coefficient of reflection at the cathode: $R = (Z_{in} - \rho_c)/(Z_{in} + \rho_c)$. Since $|R|^2$ is the probability of particle reflection and the number of particles remains constant, the transparency is determined as $D = 1 - |R|^2$. A more sophisticated matrix method for independent determination of R and D was used in [3]. A stepwise approximation of $V(s)$ with 200 sections was used for numerical calculations. The exact formula of function $V(s)$ in the case of two electrodes (cathode at $s = 0$ and anode at $s = d$) was approximated using the expression from [3,4] $V_0(z) \approx E_{Fc} + W_c(1 - \alpha/d)[1 - (2z/d - 1)^4]/\varepsilon$ and a more accurate expression

$$V_0(z) \approx E_{Fc} + W_c \frac{(1-\alpha/d)(1+\delta_c/d)^2}{\varepsilon(1-\delta_c/d)^2} \times \left[1 - \frac{\delta_c/d}{\big(z + \delta_c(1-z/d)\big)\big(d - z + \delta_c z/d\big)}\right]. \quad (2)$$

They were obtained for a flat cathode and anode made of the same material (i.e., with identical work functions (WFs) $W_c = W_a$) for coordinate $z = s$ normal to the surfaces. Formula (2) with the appropriate substitutions was also used for the grid–anode gap.. Thus, $\delta_c = 1/(16\pi\varepsilon_0 W_c)$. Constant α corresponds to the Schottky effect and assumes a value of $\alpha \approx 2.731\delta_c$. With WF $W_c = 3.6$ eV, $\delta_c = 0.1$ nm. This is the characteristic distance at which the image forces become inactive. Formula (2) is fairly accurate for narrow and wide barriers and defines symmetrical barrier $V_0(0) = V_0(d) = E_{Fc}$ with a maximum height of $V_0(d/2) = E_{Fc} + W_c(1 - \alpha/d)/\varepsilon$, which is approximately equal to $E_{Fc} + W_c/\varepsilon$ for wide barriers. Other parabolic approximations (Fig. 2, *b*) are less accurate (exact results are denoted with asterisks). The formulae correspond to the potential measured relative to the bottom of the cathode conduction band. If the anode voltage is nonzero, formula $V(z) = V_0(z) - eU_a z/d$ should be used for the potential. The barrier then becomes asymmetric. In the case of a vacuum diode, one needs to set $\varepsilon = 1$. We used formula $V(s) = V_0(s) - eU_a s/d(z)$ for the cathode–grid gap at $\varepsilon = 5$, $s = x$ (vertical coordinate in Fig. 1), and $d(z) = t_d$ and the grid–anode gap with $\varepsilon = 1$ on the assumption that $s \approx z'$ is the current coordinate along the trajectory and $d(z) = l_c + l_a - z$, where z is the coordinate tied to the origin of the trajectory and specifying transparency $D(E, z)$ along it. With the transparency values determined, the current was calculated using formula (1). Thus, the anode–grid potential is $V_a(z') = -eU_g - e(U_g - U_a)z'/(l_c + l_a - z)$. The approximation becomes more accurate as l_a increases; its error at $t_d/l_c \ll 1$ is on the order of l_c/l_a. A more accurate treatment of trajectory lengths leads to complex formulae. The values of $l_c = 100$ nm, $w = 10\,\mu$m, $l_a = 1000$ nm, $U_g = 5$ V, $U_a = 1500$ V, $t_d = t_g = 2$ nm, $W_c = W_a = 4.36$ eV, and $E_{Fc} = E_{Fa} = 7$ eV (copper) were used to estimate the current. Figure 2 shows the quantum potential profiles in the initial sections (within 10 nm) for different voltages, sizes, and emission points (*a*) and a comparison of the approximations of V (*b*). It can be seen that the shape of potential $V(s)$ between the cathode and the grid is governed by the grid voltage, while the shape grid–anode potential is set by the anode voltage and the grid–anode distance, which specify the slope and length of a nearly triangular barrier. An electron moves quasi-classically in the sloped region, but the phase incursion in the wave function is accurately accounted for in the SE solution. At a large grid–anode distance, the barrier transparency values corresponding to different emission points are virtually equal, simplifying the calculation of the current.

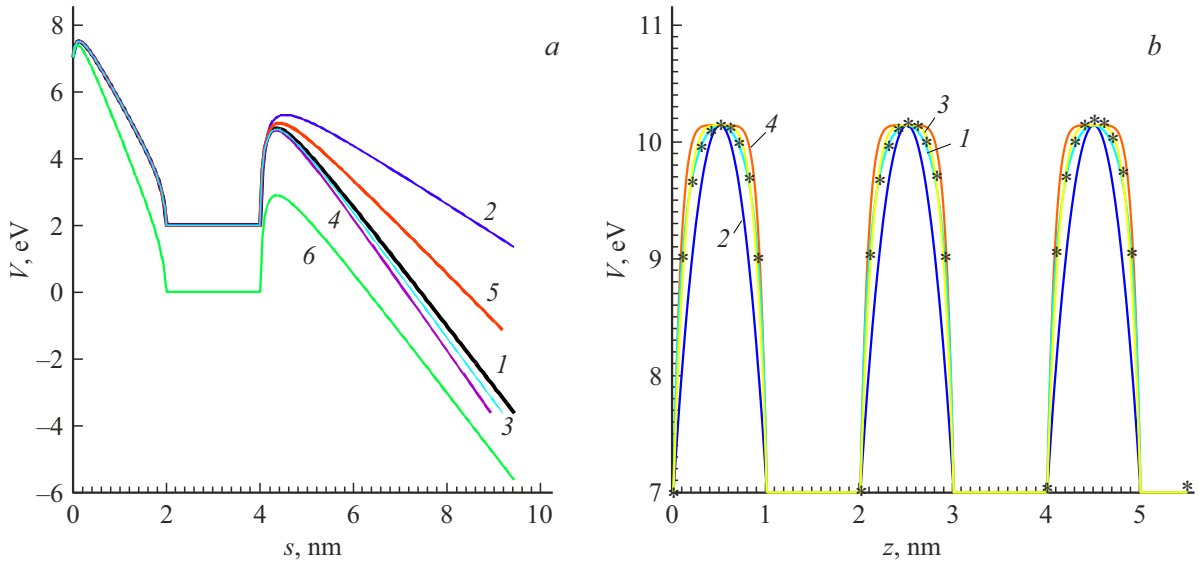

Figure 2. *a* — Distribution of quantum potential V in the structure shown in Fig. 1 along the trajectories with distance s from the emission point. $t_d = t_g = 2$ nm, $\varepsilon = 5$ at $U_g = 5$ (*1*–*5*) and 7 V (*6*) for the structure with $l_c = 10$ nm, $l_a = 100$ nm (*1*–*4*, *6*) and the structure with $l_c = 100$ nm, $l_a = 1000$ nm (*5*). Voltages $U_a = 200$ (*1*, *3*, *4*, *6*), 100 (*2*), and 1500 V (*5*) were set. Curves *1*, *2*, *5*, *6* were plotted for emission point $z = 0$; curve *3*, for $z = l_c/2$; curve *4*, for $z = l_c$. *b* — Approximation of the variation of quantum potential V with length z in a resonant tunneling structure with two wells according to formula (5) (curve *1*) and by parabolas of the second (*2*), fourth (*3*), and sixth (*4*) orders. $t_d = t_g = 1$ nm, $U_g = U_a = 0$, and $\varepsilon = 1$. $E_{Fc} = 7$ eV and $W_c = 4.36$ eV in both panels.

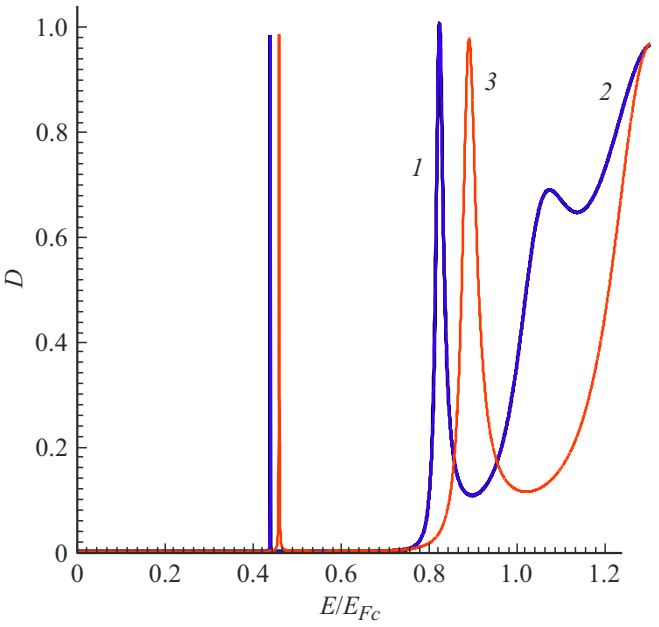

Figure 3. Transparency D as a function of ratio E/E_{Fc} for potential configurations represented by curves *1* (*1*) and *6* (*2*) in Fig. 2, *a*. Line *3* corresponds to curve *4* in Fig. 2, *a* with a platinum grid used.

Figure 3 shows the transparency of barriers for curves *1* and *6* in Fig. 2, *a* (lines *1* and *2*, respectively) and curve *4* in Fig. 2, *a* with a platinum grid used (line *3*; the WF is 5.5 eV). Integration in (1) was performed by the Simpson method with the use of several thousand points, which provides high accuracy. The formulae for resonant frequencies and quality factors were given in [3,10], and the authors of [10] have isolated resonance regions in the integral in the form of a sum with integration over a region without resonances. The current–voltage curves are close to similar curves for nanostructures presented in [3,4]. The barrier heights (curve *1* in Fig. 2, *a*) for the copper grid are not aligned. When a platinum grid with a WF of 5.5 eV is used instead of the copper one, the second barrier gets raised by 1.2 eV, and the current increases significantly. The calculated current value is $I = 12.1$ A (for curve *5* in Fig. 2, *a*, $w = 100\,\mu$m). This is a fairly strong current for an emission nanostructure with a beam power of 18 kW. It may be raised via a several-fold increase in voltage at the second anode; a relativistic beam may be obtained in this case. The interelectrode distance may also be increased several times by focusing the beam with a strong magnetic field. A tightly focusing field has an estimated strength of the order of 1 T. In the considered structure, the grid actually serves as the first accelerating electrode, and the anode is the second electrode. The beam current may be adjusted by varying the grid voltage. It is impractical to alter the anode voltage, since the anode and the focusing electrode voltages in the structure (Fig. 1) are instrumental to ensuring the beam passage. The main problem is synthesis of the electrode configuration of the electron-optical system. It is convenient to set $U_g \geqslant E_{Fc}$ to secure the possibility of tunneling of electrons with an arbitrary energy at the cathode. In a similar vein, one may consider resonant tunneling with a double or even multi-electrode grid, but, in order to ensure

ballistic transport, the overall size should not exceed 10 nm, which makes it impossible to use more than three or four electrodes. The use of a quasi-periodic Bragg superlattice with a large number of electrodes (quantum wells) and the production of a wide resonant tunneling region require low temperatures.

Thus, a field emission structure with an atomically smooth emitting surface and a pulling grid with a high-current high-power ribbon electron beam for pulsed TWTs operating in the millimeter and terahertz ranges and other applications was proposed. The grid protects the cathode from ion bombardment and allows one to modulate the beam current with a low voltage on the order of a few volts.

Funding

This study was supported financially by the Ministry of Education and Science of the Russian Federation as part of the state assignment (No. FSRR-2023-0008).

Conflict of interest

The author declares that he has no conflict of interest.

References

[1] A.A. Burtsev, Yu.A. Grigor'ev, A.V. Danilushkin, I.A. Navrotskii, A.A. Pavlov, K.V. Shumikhin, Tech. Phys., **63** (3), 452 (2018). DOI: 10.1134/S1063784218030040.
[2] *Sverkhshirokopolosnye lampy begushchei volny. Issledovanie v SVCh-, KVCh- i TGCh-diapazonakh. Vnedrenie v proizvodstvo*, Ed. by N.A. Bushuev (Radiotekhnika, M., 2015) (in Russian).
[3] M.V. Davidovich, I.S. Nefedov, O.E. Glukhova, M.M. Slepchenkov, J. Appl. Phys., **130** (20), 204301 (2021). DOI: 10.1063/5.0067763
[4] M.V. Davidovich, Tech. Phys., **67** (9), 1196 (2022). DOI: 10.21883/TP.2022.09.54684.257-21.
[5] J. Robertson, Sci. Eng. R: Reports, **37** (4-6), 129 (2002). DOI: 10.1016/S0927-796X(02)00005-0
[6] D. Sunil, V.D. Vankar, K.L. Chopra, J. Appl. Phys., **69** (6), 3719 (1991). DOI: 10.1063/1.348464
[7] E.A. Il'ichev, A.E. Kuleshov, G.N. Petrukhin, P.V. Minakov, G.S. Rychkov, V.V. Sen', E.G. Teverovskaya, Tech. Phys. Lett., **47**, 503 (2021). DOI: 10.1134/S1063785021050230.
[8] M.V. Davidovich, R.K. Yafarov, in *2017 Radiation and scattering of electromagnetic waves (RSEMW)* (IEEE, 2017), p. 384–387. DOI: 10.1109/RSEMW.2017.8103680
[9] M.V. Davidovich, R.K. Yafarov, Tech. Phys., **64** (8), 1210 (2019). DOI: 10.1134/S106378421908005X.
[10] M.V. Davidovich, I.S. Nefedov, O.E. Glukhova, M.M. Slepchenkov, J.M. Rubi, Sci. Rep., **13**, 19365 (2023). DOI: 10.1038/s41598-023-44900-2

Translated by D.Safin